

# Very High-Quality Single-Walled Carbon Nanotubes Grown Using a Structured and Tunable Porous Fe/MgO Catalyst

Jingqi Nie, Weizhong Qian,\* Qiang Zhang, Qian Wen, and Fei Wei

Beijing Key Laboratory of Green Reaction Engineering and Technology and Department of Chemical Engineering, Tsinghua University, Beijing, 100084, People's Republic of China

Received: May 14, 2009; Revised Manuscript Received: October 14, 2009

Fe/MgO nanoparticle catalysts were prepared and used to grow single-walled carbon nanotubes (SWCNTs) from the decomposition of methane. The porous structure of the catalyst can be tailored by an ethanol–thermal treatment and calcination. Catalysts with sufficiently large pores (50 nm to 5  $\mu$ m) can produce very high-quality SWCNTs that had an intensity ratio of D band to G band in their Raman spectra of less than 0.02–0.03. These SWCNTs had fewer defects than any other SWNT products from the chemical vapor deposition process previously reported.

## Introduction

The ideal single-walled carbon nanotube (SWCNT) is a rolled graphite layer that is a perfect structure without structural defects.<sup>1</sup> However, SWCNTs prepared by arc discharge,<sup>2–4</sup> laser ablation,<sup>5</sup> and chemical vapor deposition (CVD)<sup>6–10</sup> all have defects. These defects included amorphous carbon present inside or outside the CNT wall and intrinsic defects in the CNT carbon layer.<sup>11,12</sup> These defects degrade the mechanical, electrical, and thermal conductive properties of the SWCNTs.<sup>13–15</sup> The resonant Raman scattering method has been established to evaluate these defects.<sup>7,16–19</sup> The intensity ratio of the D band to G band ( $I_D/I_G$ ) in a Raman spectra is used to characterize the amount of defects in the SWCNTs. Histograms reported in many works indicate that the  $I_D/I_G$  values are, in most cases, smaller than 0.02 for SWCNTs produced by the arc discharge and laser ablation methods<sup>4,5,16</sup> but were all larger than 0.08–0.1 for SWCNTs produced by the CVD process.<sup>7,16–23</sup> It has been difficult to improve the  $I_D/I_G$  ratio obtained in the CVD process despite the many attempts made, for example, by varying the catalysts (metals, such as Co, Fe, Ni, Mo, etc. and their alloys, and the supports, such as alumina, silica, MgO, and other supports/substrates),<sup>6,7,24</sup> carbon sources (hydrocarbons, CO, ethanol, etc. mixed with various inert gases and/or H<sub>2</sub>),<sup>25</sup> temperature,<sup>26</sup> and pressure. On the other hand, the CVD method has advantages over the arc discharge and laser ablation methods in the use of mild growth conditions, its potential for scale up production, and the selectivity to SWCNTs. Thus, a challenge is how to prepare very high-quality SWCNTs (those that have very few defects) by the CVD method.

Three factors determine that the formation of defects in the SWCNTs from the CVD method is more probable than from the other methods. First, a local high-temperature condition, such as that present in the arc discharge and laser ablation processes, is needed for good crystallization of SWCNTs.<sup>4,5,16</sup> Therefore, the defects in the SWCNTs produced by these two methods are less than those from CVD.<sup>7,10,16–22</sup> It has been noted that the SWCNT products from the CVD method assisted by a laser still had relatively high  $I_D/I_G$  values (0.08–0.1),<sup>27</sup> which further suggested that the defects in the SWCNTs were more sensitive

to the temperature than to the other parameters. Second, in the arc discharge and laser ablation processes, the formation of a SWCNT only needs to break a carbon–metal bond. In comparison, it is not only the carbon–metal bond but also the metal–support interaction bond that both have to be broken for the lifting of the SWCNTs in the CVD process.<sup>28</sup> In situ TEM observations have confirmed that a large stress is produced in the lifting of CNTs from metal nanoparticles (NPs), which resulted in the formation of defective and curved products.<sup>29,30</sup> Third, SWCNTs grow freely in the chamber of the arc discharge and laser ablation reactor, where the concentrations of gas and solid are both very low. Similarly, in some special CVD processes, superlong SWCNTs with very few defects have been grown freely in a floating gas<sup>31</sup> or in a liquid phase.<sup>32</sup> However, for most CVD processes, the SWCNTs grow surrounded by many stacked catalyst particles. Much evidence has suggested that, for the growth of multi-walled, double-walled carbon nanotubes (MWCNTs, DWNCNTs) and SWCNTs over porous catalysts,<sup>11,20,21,33</sup> the limited size of the catalyst pore hindered the growth of the CNTs and contributed significantly to the appearance of defects. To improve the situation, a rational catalyst structure design can be used.

In the present work, nanosized Fe/MgO particles were used for the growth of SWCNTs, in place of the bulk of large porous catalyst powder particles. The idea was to allow the SWCNTs to grow freely without touching the walls in the pores in the bulk of porous particles.<sup>11,20,21,33</sup> Unfortunately, even in the use of nonporous nanosized particles, there was an unavoidable aggregation of the catalyst NPs in the drying and calcination of the catalysts,<sup>34–36</sup> which still resulted in the formation of a porous catalyst structure with large pores of up to several ten micrometers. Thus, an ethanol–thermal treatment of the catalyst was further used to reduce the surface energy during evaporation to inhibit the densification of the catalyst agglomerate during the drying and calcination. As a result, a porous Fe/MgO architecture with sufficient large pores of 50 nm to 5  $\mu$ m was created, which allowed the growth of SWCNTs with an  $I_D/I_G$  ratio that was decreased to 0.03 (and even to 0.01). Compared with the SWNTs produced using a bulk Fe/MgO catalyst that is a porous powder, the defects in the SWCNTs were decreased by 50–70%. The as-grown SWCNTs had fewer defects than any of the products obtained from the CVD process to date.

\* To whom correspondence should be addressed. E-mail: qianwz@mails.tsinghua.edu.cn.

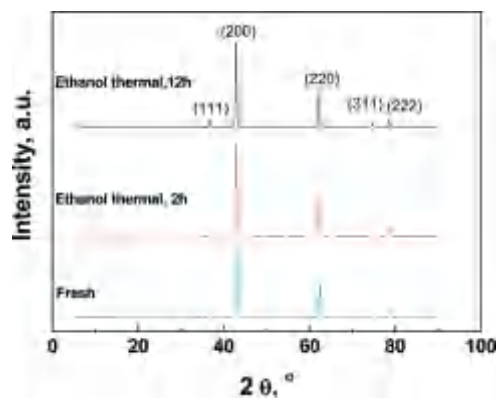


Figure 1. XRD patterns of catalysts with different treatments.

### Experimental Section

The Fe/MgO catalysts were prepared by a typical impregnating method, both with and without an ethanol–thermal treatment. The MgO NPs by the coprecipitation method (S1; see the Supporting Information) were immersed into the Fe(NO<sub>3</sub>)<sub>3</sub>–ethanol solution (ratio of Fe(NO<sub>3</sub>)<sub>3</sub> to ethanol was 1 g to 10 mL) and subjected to a 30 min ultrasonic treatment to become a gel. The gel was ethanol–thermal treated in a sealed autoclave (with its inner wall coated by a Teflon layer; the total volume was 70 mL with 50 mL of Fe/MgO–ethanol solution) at 200 °C for 2–12 h. After cooling the autoclave to ambient condition, the gel was dried at 110 °C for 24 h and calcined at 900 °C for 1 h. The loading of iron on the MgO support was controlled from 0.07 to 0.3 wt %. The reference catalyst used, without an ethanol–thermal treatment, was called a fresh catalyst. Its preparation followed the same procedure except that a Fe(NO<sub>3</sub>)<sub>3</sub> aqueous solution was used without the hydrothermal treatment. For comparison, a catalyst was further calcined at 900 °C<sup>10</sup> for 3 h after the ethanol–thermal treatment.

To grow SWCNTs, 0.05 g of catalyst was put into a horizontal quartz reactor (30 mm i.d.) and heated to 800 °C in Ar for 2 h. A mixture of CH<sub>4</sub>/H<sub>2</sub>/Ar (flow rate of 80, 5, and 400 mL/min, respectively) was then fed into the reactor for 2–15 min. After cooling in Ar to ambient condition, the SWCNTs were sampled and characterized by transmission electron microscopy (TEM, JEOL2010, 200 kV), thermogravimetric analysis (TGA, TA2050, 20–900 °C, 15 °C/min), and resonant Raman spectroscopy (Renishaw, RM2000, He–Ne laser excitation line at 633 and 514 nm). Different catalysts are characterized by X-ray diffraction (XRD, D/MAX-III A, nickel-filtered Cu Kα radiation, 3–90°), TEM (JEOL, at 200 kV), mercury porosimetry (MP, AutoPore II 9220 V3.04), temperature-programmed reduction (TPR), X-ray photoelectron spectroscopy (XPS, PHI Quantera SXM, 3.4 × 10<sup>−9</sup> Torr), and nitrogen adsorption isotherm characterization (Autosorb-1-C).

### Result and Discussion

The catalyst before reaction showed only the peak of the MgO crystallites in the XRD pattern (Figure 1). The low loading of Fe was too low to detect. The size of the catalyst NPs, calculated from the MgO (220) peak, was 37.7 and 48.3 nm for the samples without and with the ethanol–thermal treatment of 2 h, respectively. No peak at 26° was observed in the XRD pattern, which showed the pristine catalyst did not contain coke or carbon species that were possible from the decomposition of ethanol. Thus, we can take it that the decreased defect formation on these SWCNTs (discussed later) was not due to the formation of some other active phase, for example, iron carbide. XPS

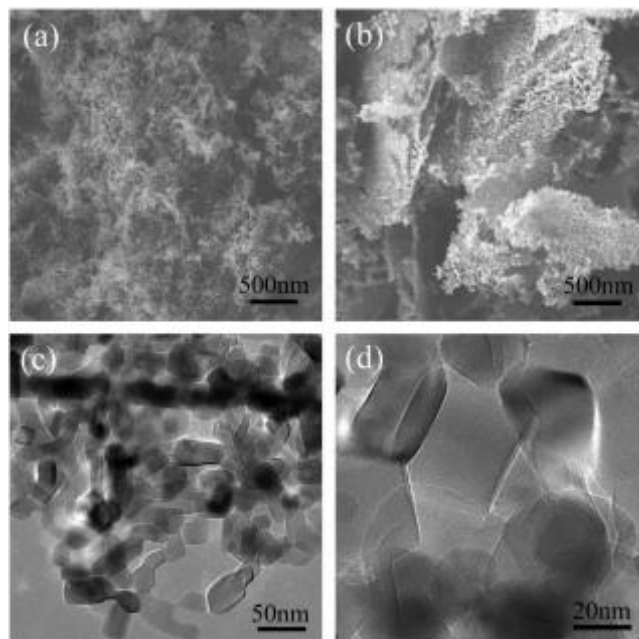
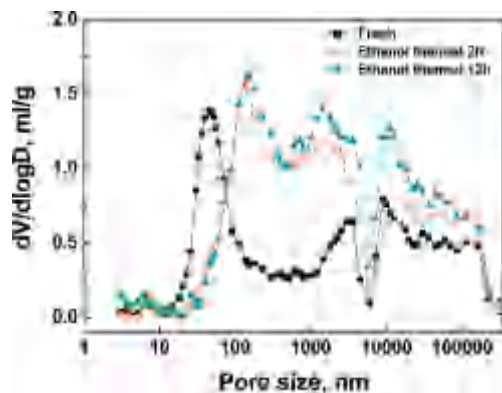


Figure 2. SEM and TEM images of catalysts without (a, c) and with the ethanol–thermal treatment (b, d).

characterization (Figure S1; see the Supporting Information) indicated that there was a very weak signal of an iron species on the surface of the fresh catalyst and no detectable iron species on the catalyst with the ethanol–thermal treatment. These results suggested that, before the reaction, the iron species was dispersed uniformly in the MgO matrix of the catalyst and did not form iron clusters.<sup>10</sup>

SEM images (Figure 2a,b) indicated that both catalysts were NPs that formed large aggregates with obvious large holes and vacancies. The TEM images (Figure 2c,d) showed that the individual particle had well-defined crystalline facets and the size of the MgO particles was in agreement with the XRD data. Fe NPs, which would be a deep black color in TEM images, were not observed on the catalyst before reaction, in agreement with the XPS result that the Fe oxide was uniformly distributed in the MgO phase.<sup>10</sup> TPR characterization for the different catalysts (Figure S2; see the Supporting Information) indicated that the fresh catalyst had three reduction peaks at 350, 500, and 640 °C, which were assigned to Fe<sub>2</sub>O<sub>3</sub>, Fe<sub>3</sub>O<sub>4</sub>, and FeO, respectively.<sup>37</sup> The ethanol–thermal treated catalyst only had the reduction peaks of Fe<sub>3</sub>O<sub>4</sub> at 400 °C and FeO at 580 °C. These results suggested that the temperature needed to form Fe clusters is higher than 580–600 °C. However, although no iron cluster was formed during the catalyst preparation, the drying at 110 °C for the catalyst precursor did result in the aggregation of the catalyst particles, which was driven by forces in the evaporation of water or ethanol.<sup>34–36</sup> The subsequent calcination at 900 °C sintered the catalyst particles into a three-dimensional porous structure, which was stable and which was not destroyed by the 30 min ultrasonic treatment for TEM characterization (Figure 2c,d).

The pore size distribution of the different catalysts was characterized by N<sub>2</sub> adsorption (Figure S3; see the Supporting Information) and Hg penetration (Figure 3). The ethanol–thermal treatment increased the percentage of pores that were in the 2–10 nm and 50 nm–5 μm ranges but decreased the percentage of pores that were in the 10–50 nm range, as compared with those of the fresh catalyst. The percentage of the pores that were 50 nm to 5 μm increased 3-fold and could be further increased



**Figure 3.** Pore size distributions of catalysts with different treatments.

with an increased ethanol–thermal treatment time. These pores were mainly the inner pores of the catalyst architecture, whereas the much larger pores of 5–300  $\mu\text{m}$  were due to the stacking vacancies between catalyst aggregates. In agreement with the latter assignment, the percentage of these latter pores (5–300  $\mu\text{m}$ ) did not vary insignificantly for the three catalysts. The effect of the ethanol–thermal treatment on the catalyst structure was similar to other hydrothermal<sup>38</sup> or solvent–thermal processes. Generally, some MgO particles are dissolved in the ethanol solution and then recrystallized.<sup>22,39,40</sup> With a short treatment time (2 h), the dissolved MgO was present in a small amount and the recrystallization over the undissolved relatively large seeds resulted in the formation of relatively large MgO NPs. However, a long treatment time (12 h) caused a large amount of MgO NPs to dissolve, which produced small MgO NPs upon recrystallization due to the increased supersaturation of MgO in ethanol. In the following drying process, the evaporation of ethanol still caused the catalyst particles to aggregate. However, compared with the use of water evaporation, the smaller surface energy during ethanol evaporation resulted in the formation of a relatively loosely packed porous structure with many large pores in the range of 50 nm to 5  $\mu\text{m}$ .

For the growth of SWCNTs, most Fe oxide species were first reduced to Fe NPs 1–3 nm in diameter (Figure 4). SWCNTs grow on the Fe NPs dispersed on the surface of the catalyst particles (Figure 4b,c). Because the catalyst has a three-dimensional porous structure, the SWCNTs first to be grown inside the catalyst follow a random direction. Therefore, the growth of relatively long SWCNTs will be obstructed by the catalyst wall regardless of the growth direction and they get bent. Depending on the growth position of the SWCNTs inside the catalyst, some get twisted together inside the limited pore space when these pores are less than 50 nm to 5  $\mu\text{m}$  and would cease to grow,<sup>21</sup> while some other SWCNTs would alter the growth direction (along the surface of or around the catalyst particles, as shown in Figure 4d,e) and significant defects get produced in the curved sections of the SWCNTs. However, some SWCNTs also get to grow straight through the pore of the catalyst structure (Figure 4f). The growth out of the catalyst structure is free, and many small such SWCNT bundles can form a large bundle (Figure 4g,h). It can be suggested that the complex porous catalyst structure has a pronounced influence on the quality of the SWCNTs. A catalyst structure with sufficiently large pores (e.g., those from the ethanol–thermal treatment) gives advantages over the fresh catalyst in growing clean and long SWCNTs in large amounts with few defects, as shown in Figure 5.

Raman characterization of the SWCNTs at different times provided evidence of the confined growth process (Figure 6).

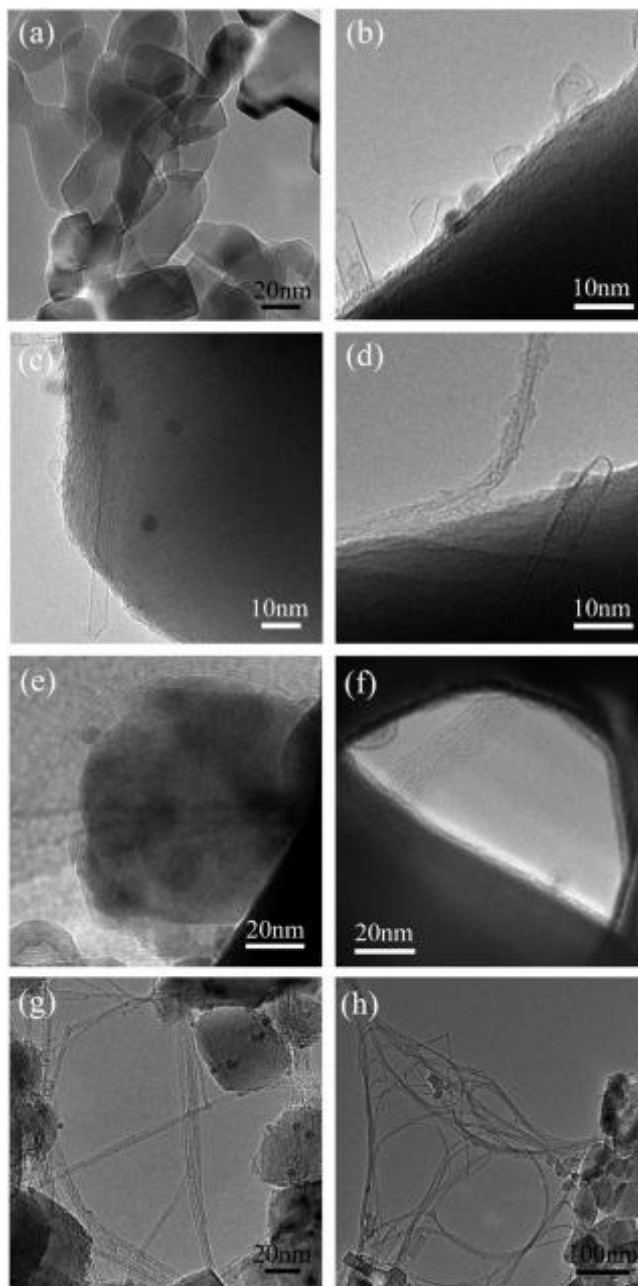


**Figure 4.** TEM images of SWCNTs from catalysts with different treatments. (a) Highly aggregated catalyst structure that was not destroyed by an ultrasonic treatment. (b) Initial growth of SWCNTs on the catalyst. (c) Short SWCNTs grown that adhere on the surface of the catalyst. (d) Long SWCNTs obstructed by the catalyst particles, which were bent and that continued to grow on the catalyst surface. (e) Long SWCNT bundles grown along the surface of catalyst particles. (f) Long straight SWCNT bundles grown through the large pores of the aggregated catalyst structure. (g) Many SWCNT bundles grown around catalyst particles in different growth directions. (h) Large amounts of small SWCNT bundles that form a large bundle growing out of the catalyst structure.

The initially grown SWCNTs had the highest  $I_D/I_G$  value. This was because they had to break the metal–support interaction bond and the carbon–metal bond. After that, the SWCNTs grew freely inside the porous catalyst architecture and the amount of defects decreased to some extent. However, after 30 s of growth, the  $I_D/I_G$  value of the SWCNTs increased with growth time. This reversed trend in the  $I_D/I_G$  value with time was observed using different Raman laser excitations at 633 and 514 nm for SWCNTs with different diameters. The formation of amorphous

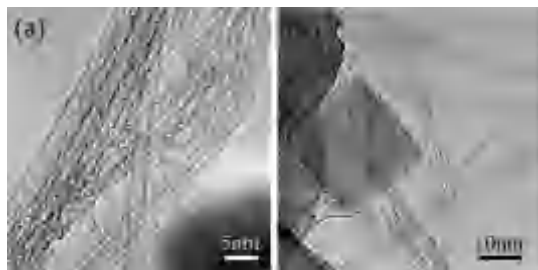


**Figure 5.** Magnified TEM images of SWCNTs from the catalyst without (a) and with (b) ethanol-thermal treatment.

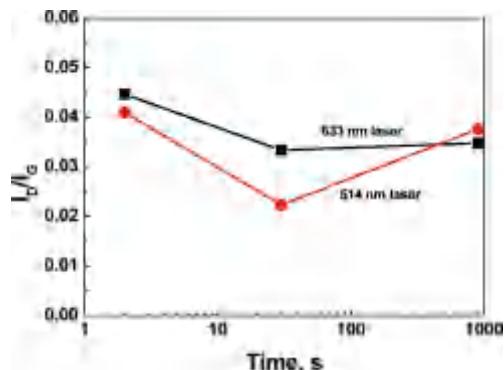


**Figure 6.** Evolution of the  $I_D/I_G$  ratio of SWCNTs with growth time (from the 2 h ethanol-thermal treated catalyst).

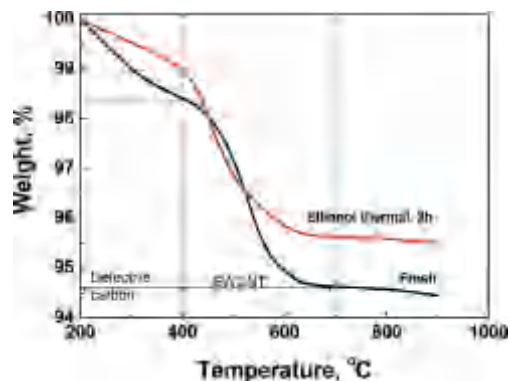


**Figure 7.** TGA pattern of SWCNTs from catalysts with different treatments.

carbon, carbon-encapsulated metal NPs, or the deformation of the SWCNTs can all be the cause of the increased  $I_D/I_G$  value. To distinguish between these, TGA analysis was used to characterize the existence of defective amorphous carbon or SWCNTs using their different oxidative thermal behavior. As shown in Figure 7, the yields of carbon were 5.56 and 4.50% over the fresh and ethanol-thermal treated Fe/MgO catalysts, respectively. No further weight loss was observed after 600 °C, which suggested that all the carbon products were free of MWCNTs and carbon-encapsulated metal NPs. The weight loss before 400 °C was attributed to the burning of amorphous carbon or defective carbon. Thus, the ratio of SWCNTs to defective amorphous carbon can be determined. This was 2.31 and 3.5 for the carbon samples over the fresh and the ethanol-thermal treated catalyst, respectively. Because the content of amorphous carbon from the thermal decomposition of  $\text{CH}_4$  was nearly the same for the different catalysts, the contribution of amorphous carbon to the  $I_D/I_G$  values should not change with reaction time. From the above analysis, we can say that the increased  $I_D/I_G$  value with reaction time was due to the deformation (bending) of long SWCNTs due to obstruction by the catalyst wall.

In addition, the TPR result (Figure S2; see the Supporting Information) suggested that, as compared with the fresh catalyst, the Fe NPs after the ethanol-thermal treatment became more uniform, but the reducible amount was significantly decreased. This result explained why the yield of carbon from the ethanol-thermal treated catalyst was lower, as shown in Figure 7. On the other hand, from comparing the ratio of SWCNTs to defective carbon over the different catalysts, it can be deduced that SWCNTs grew faster on the ethanol-thermal catalyst than on the fresh catalyst. This assumed that the same amount of amorphous carbon was produced from the thermal decomposition of  $\text{CH}_4$  in the same time. This is reasonable because the large pores of the catalyst with the ethanol-thermal treatment allowed the quick growth of SWCNTs; that is, the higher percentage of large pores of 50 nm to 5  $\mu\text{m}$  in the catalyst increased the ratio of SWCNTs growing out of the catalyst structure. These can further grow to a length that was not possible in the pores of the host catalyst.

The Raman spectra of the SWCNTs in Figure 8a at 633 nm and Figure 8b at 514 nm both suggested that there was a very strong radial breathing mode (RBM) response at 100–250  $\text{cm}^{-1}$ . The dominant products were 1.26 nm tubes with a RBM peak centered at 190  $\text{cm}^{-1}$ . All the samples had a very strong G band ( $\sim 1589 \text{ cm}^{-1}$ ) and very weak D band ( $\sim 1310 \text{ cm}^{-1}$ ). The  $I_D/I_G$  data in Figure 8a,b indicated that the amount of defects in the SWCNTs was very small when grown in the catalyst with the ethanol-thermal treatment, but this was not the case with the fresh catalyst. This result is qualitatively in agreement with the ratio of SWCNT to defective carbon in the TGA results (Figure 7). Further investigation indicated that the  $I_D/I_G$  values did not change significantly with the metal loading of the catalyst. The change due to this was small compared with the change due to whether the preparation method was with or without the ethanol-thermal treatment (Figure 8c). We also tested the effect of growth temperature (800, 850, 900, and 950 °C) on the growth of the SWCNTs. The  $I_D/I_G$  values did not change significantly compared to those in Figure 8c. Moreover, Figure 8d indicated that the amount of defects in the SWCNTs decreased gradually with an increase of the ethanol-thermal treatment time, which resulted in the formation of more large pores (Figure 3). The decreasing trend of the  $I_D/I_G$  value was observed with both the 633 and the 514 nm laser in the Raman characterization. Because SWCNTs with different diameters are sensitive to different Raman laser wavelengths, it is reasonable that there was minor difference in the detailed  $I_D/I_G$  value.<sup>42</sup> To provide further evidence of this effect, the catalyst after the 2 h ethanol-thermal treatment was intentionally further calcined in air at 900 °C for 3 h, which decreased the percentage of large pores. Subsequently, a high  $I_D/I_G$  value (0.048) for the SWCNTs was observed (blue triangle in Figure 8d). Most of the  $I_D/I_G$  values of the SWCNTs from the catalyst with the ethanol-thermal treatment were smaller than 0.04. The smallest value obtained was 0.018. These values were all smaller than those (mostly larger than 0.1) obtained using bulk Fe/MgO catalyst porous powder with the same Fe loading<sup>20</sup> and SWCNT samples from other catalysts in several hundred references that reported Raman data.<sup>7,10,16–22,33</sup> The SWCNTs in the present work can be ranked as the product with the fewest defects prepared by the CVD method to date, and they are comparable in being defect-free to the SWCNTs from the arc discharge method.<sup>4,5,16</sup>

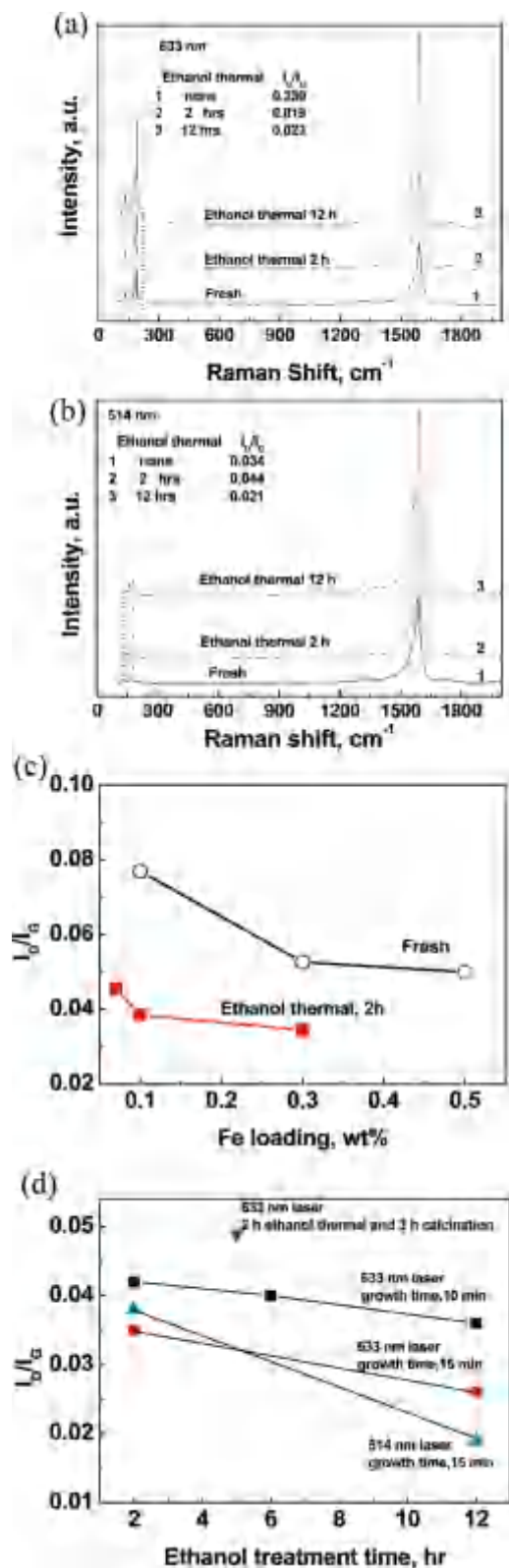


**Figure 8.** Raman spectra of SWCNTs from catalysts with different treatments: (a) Raman spectra (633 nm) and (b) Raman spectra (514 nm). (c) The effect of iron loading. (d) The effect of ethanol–thermal treatment time.

The above growth phenomenon of the SWCNTs is similar to that of MWCNTs.<sup>41</sup> However, MWCNTs with large diameters can destroy the catalyst structure in the course of their growth, but this was not the case with the SWCNTs. Also, the increase in the  $I_D/I_G$  value of the MWCNTs was less significant compared

to the SWCNTs.<sup>41</sup> Recently, a catalyst with an open microscale structure was prepared using carbon fibers as a burnable sacrificial template.<sup>42</sup> Such a catalyst increased the yield of SWCNTs but did not increase the quality of SWCNTs significantly. This was probably because the pores in that catalyst were not large enough, as was the case in the present work. These results all indicate that the quality of SWCNTs produced is sensitive to the growth condition. Our catalyst preparation method was very simple and can be easily performed on a large scale so that we can produce a much larger amount of very high-quality SWCNTs, as compared with the previous work.<sup>42</sup> Our results suggested that, if monodispersed nanosized catalyst particles can be prepared in large amounts and it can be suspended in the reactor, it should be possible to increase the quality of the SWCNTs further.

## Conclusions

In producing SWCNTs from methane decomposition using a Fe/MgO catalyst, SEM/TEM, TGA, Hg penetration, and Raman results suggested that a catalyst packing structure with large pores is crucial for the formation of SWCNTs with much fewer defects. The ethanol–thermal method is effective for increasing the percentage of very large pores in the porous catalyst structure and can be used for the growth of very high-quality SWCNTs.

**Acknowledgment.** The work was supported by the Natural Scientific Foundation of China (20606020 and 20736007), FANEDD (200548), and the China National Program (2006CB932702). The authors are grateful to Professor Dezeng Wang for English improvements.

**Supporting Information Available:** The preparation method of MgO NPs and XPS, TPR, and  $N_2$  adsorption data of the catalyst. This material is available free of charge via the Internet at <http://pubs.acs.org>.

## References and Notes

- Iijima, S.; Ichihashi, T. *Nature* **1993**, *363*, 603.
- Journet, C.; Maser, W. K.; Bernier, P.; Loiseau, A.; de la Chapelle, M. L.; Lefrant, S.; Deniard, P.; Lee, R.; Fischer, J. E. *Nature* **1997**, *388*, 756.
- Du, F.; Ma, Y. F.; Lv, X.; Huang, Y.; Li, F. F.; Chen, Y. S. *Carbon* **2006**, *44*, 1327.
- Wang, M.; Wang, X. Q.; Li, Z. H.; Liu, Z. Y.; He, P. *Mater. Chem. Phys.* **2006**, *97*, 243.
- Maser, W. K.; Munoz, E.; Benito, A. M.; Martinez, M. T.; de la Fuente, G. F.; Maniette, Y.; Anglaret, E.; Sauvajol, J. L. *Chem. Phys. Lett.* **1998**, *292*, 587.
- Cassell, A. M.; Raymakers, J. A.; Kong, J.; Dai, H. J. *J. Phys. Chem. B* **1999**, *103*, 6484.
- Li, Q. W.; Yan, H.; Cheng, Y.; Zhang, J.; Liu, Z. F. *J. Mater. Chem.* **2002**, *12*, 1179.
- Lyu, S. C.; Liu, B. C.; Lee, T. J.; Liu, Z. Y.; Yang, C. W.; Park, C. Y.; Lee, C. J. *Chem. Commun.* **2003**, 734.
- Chen, Y.; Ciuparu, D.; Lim, S.; Haller, G. L.; Pfefferle, L. D. *Carbon* **2006**, *44*, 67.
- Ning, G. Q.; Wei, F.; Wen, Q.; Luo, G. H.; Wang, Y.; Jin, Y. J. *J. Phys. Chem. B* **2006**, *110*, 1201.
- Dresselhaus, M. S.; Dresselhaus, G.; Jorio, A.; Souza, A. G.; Saito, R. *Carbon* **2002**, *40*, 2043.
- Gregan, E.; Keogh, S. M.; Maguire, A.; Hedderman, T. G.; Neill, L. O.; Chambers, G.; Byrne, H. J. *Carbon* **2004**, *42*, 1031.
- Bernholc, J.; Brabec, C.; Nardelli, M. B.; Maiti, A.; Roland, C.; Yakobson, B. I. *Appl. Phys. A: Mater. Sci. Process.* **1998**, *67*, 39.
- Jaroenapibal, P.; Luzzi, D. E.; Evoy, S.; Arepalli, S. *Appl. Phys. Lett.* **2004**, *85*, 4328.
- Lacerda, R. G.; Teh, A. S.; Yang, M. H.; Teo, K. B. K.; Rupasinghe, N. L.; Dalal, S. H.; Kozioł, K. K.; Roy, D.; Amarantunga, G. A. J.; Milne, W. I.; Chhowalla, M.; Hasko, D. G.; Wyczisk, F.; Legagneux, P. *Appl. Phys. Lett.* **2004**, *84*, 269.

- (16) Lv, X.; Du, F.; Ma, Y. F.; Wu, Q.; Chen, Y. S. *Carbon* **2005**, *43*, 2020.
- (17) Ferrari, A. C.; Robertson, J. *Phys. Rev. B* **2000**, *61*, 14095.
- (18) Shen, K.; Curran, S.; Xu, H. F.; Rogelj, S.; Jiang, Y. B.; Dewald, J.; Pietrass, T. *J. Phys. Chem. B* **2005**, *109*, 4455.
- (19) Hennrich, F.; Krupke, R.; Lebedkin, S.; Arnold, K.; Fischer, R.; Resasco, D. E.; Kappes, M. *J. Phys. Chem. B* **2005**, *109*, 10567.
- (20) Zhang, Q.; Yu, H.; Liu, Y.; Qian, W. Z.; Wang, Y.; Luo, G. H.; Wei, F. *Nano* **2008**, *3*, 45.
- (21) Liu, Y.; Qian, W. Z.; Zhang, Q.; Ning, G. Q.; Wen, Q.; Luo, G. H.; Wei, F. *Carbon* **2008**, *46*, 1860.
- (22) Ning, G. Q.; Liu, Y.; Wei, F.; Wen, Q.; Luo, G. H. *J. Phys. Chem. C* **2007**, *111*, 1969.
- (23) Zhang, Q.; Qian, W. Z.; Wen, Q.; Liu, Y.; Wang, D. H.; Wei, F. *Carbon* **2007**, *45*, 1645.
- (24) Nikolaev, P.; Bronikowski, M. J.; Bradley, R. K.; Rohmund, F.; Colbert, D. T.; Smith, K. A.; Smalley, R. E. *Chem. Phys. Lett.* **1999**, *313*, 91.
- (25) Chen, Y.; Wang, B.; Li, L. J.; Yang, Y. H.; Ciuparu, D.; Lim, S. Y.; Haller, G. L.; Pfefferle, L. D. *Carbon* **2007**, *45*, 2217.
- (26) Chen, Y.; Wei, L.; Wang, B.; Lim, S. Y.; Ciuparu, D.; Zheng, M.; Chen, J.; Zocan, C.; Yang, Y. H.; Haller, G. L.; Pfefferle, L. D. *ACS Nano* **2007**, *1*, 327.
- (27) Loffler, M.; Rummeli, M. H.; Kramberger, C.; Borowiak-Palen, E.; Klingeler, R.; Gemming, T.; Buchner, B.; Pichler, T. *Chem. Mater.* **2008**, *20*, 128.
- (28) Ago, H.; Nakamura, K.; Uehara, N.; Tsuji, M. *J. Phys. Chem. B* **2004**, *108*, 18908.
- (29) Helveg, S.; Lopez-Cartes, C.; Sehested, J.; Hansen, P. L.; Clausen, B. S.; Rostrup-Nielsen, J. R.; Abild-Pedersen, F.; Norskov, J. K. *Nature* **2004**, *427*, 426.
- (30) Lin, M.; Tan, J. P. Y.; Boothroyd, C.; Loh, K. P.; Tok, E. S.; Foo, Y. L. *Nano Lett.* **2007**, *7*, 2234.
- (31) Jin, Z.; Chu, H. B.; Wang, J. Y.; Hong, J. X.; Tan, W. C.; Li, Y. *Nano Lett.* **2007**, *7*, 2073.
- (32) Jeong, S. H.; Ko, J. H.; Park, J. B.; Park, W. J. *J. Am. Chem. Soc.* **2004**, *126*, 15982.
- (33) Wen, Q.; Qian, W. Z.; Wei, F.; Liu, Y.; Ning, G. Q.; Zhang, Q. *Chem. Mater.* **2007**, *19*, 1226.
- (34) An, L.; Owens, J. M.; McNeil, L. E.; Liu, J. *J. Am. Chem. Soc.* **2002**, *124*, 13688.
- (35) Zhou, Y. C.; Rahaman, M. N. *J. Mater. Res.* **1993**, *8*, 1680.
- (36) Azuma, Y.; Shimada, M.; Okuyama, K. *J. Chem. Eng. Jpn.* **2005**, *38*, 516.
- (37) Munteanu, G.; Ilieva, L.; Andreeva, D. *Thermochim. Acta* **1997**, *291*, 171.
- (38) Dawson, W. *J. Am. Ceram. Soc. Bull.* **1988**, *67*, 1673.
- (39) Kumar, A.; Kumar, J. *J. Phys. Chem. Solids* **2008**, *69*, 2764.
- (40) Zdrzil, M. *Catal. Today* **2003**, *86*, 151.
- (41) Qian, W. Z.; Liu, T.; Wei, F.; Wang, Z. W.; Luo, G. H.; Yu, H.; Li, Z. F. *Carbon* **2003**, *41*, 2613.
- (42) Irurzun, V. M.; Tan, Y. Q.; Resasco, D. E. *Chem. Mater.* **2009**, *21*, 2238.